# Orientational Order of Fluorinated Mesogens Containing the 1,3,2-Dioxaborinane Ring: A Multidisciplinary Approach

**S. Borsacchi,[†] L. Calucci,*[,‡] J. Czub,[§] R. Dabrowski,[||] M. Geppi,*[,†] W. Kuczyński,[⊥] A. Marini,[†,#] B. Mennucci,[†] and S. Urban[§]**

*Dipartimento di Chimica e Chimica Industriale, Università di Pisa, via Risorgimento 35, 56126 Pisa, Italy, Scuola Normale Superiore, Piazza dei Cavalieri 15, 56126 Pisa, Italy, Istituto per i Processi Chimico Fisici del CNR, via G. Moruzzi 1, 56124 Pisa, Italy, Institute of Physics, Jagellonian University, Reymonta 4, 30-059 Kraków, Poland, Institute of Molecular Physics, Polish Academy of Sciences, Smoluchowskiego 17, 60179 Poznań, Poland, and Institute of Chemistry, Military University of Technology, 00-908 Warszaw, Poland*

*Received: August 26, 2009; Revised Manuscript Received: October 1, 2009*

Orientational order properties of two fluorinated liquid crystals containing the 1,3,2-dioxaborinane ring have been investigated by means of optical, dielectric, and $^{13}C$ and $^{19}F$ NMR spectroscopies. The optical birefringence and dielectric anisotropy values determined in the mesomorphic phases were analyzed in terms of well-established theoretical models to obtain the order parameters relative to the principal axis of the polarizability tensor and molecular dipole moment, respectively. A large set of data, including $^{13}C$ and $^{19}F$ chemical shift anisotropies and $^{13}C-^{19}F$ and $^{1}H-^{19}F$ couplings relative to nuclei on the aromatic rings, was acquired in the NMR experiments and analyzed to determine local order parameters (principal order parameter and biaxiality) for different rigid fragments of the mesogen aromatic core using advanced DFT methods for the calculation of geometrical parameters and chemical shift tensors. A critical analysis of the dependence of the order parameters on the data set employed and on the theoretical assumptions and approximations has also been performed. The orientational order parameters obtained using the different techniques are compared and discussed in relation to the reference frame associated with the anisotropic properties monitored.

## Introduction

In virtue of their wide nematic ranges, low rotational viscosity and conductivity properties, and high dielectric anisotropies, fluorinated liquid crystals (F-LCs) constitute an interesting class of materials for application in liquid-crystal displays (LCDs),[1] some of the properties being tailored by choosing the position of the fluorine atom(s) in the molecular structure.[2,3] Moreover, their relatively good chemical and photochemical stabilities, specific resistivities, and voltage holding ratios render these materials reliable for technical applications. In particular, it was recently shown that F-LCs belonging to a phenyl-4-(5-alkyl-1,3,2-dioxaborin-2-yl)benzoate homologous series[4] exhibit a crossover in the sign of the dielectric anisotropy in the megahertz range,[5] thus potentially allowing their use as dual-frequency materials.

The anisotropy of the physical macroscopic properties determining the possible applications of F-LCs is strongly dependent on the orientational order of the molecules within the mesophases; in this respect, a quantitative investigation of the orientational order can provide fundamental information on the mesophase structural features at the basis of LC technology. Different techniques allow orientational order parameters to be determined in liquid-crystalline phases by exploiting different anisotropic properties, these parameters being inherently dependent on the technique and, in particular, on the chosen reference frame. In two previous studies on F-LCs, we performed accurate comparisons of order parameters determined by means of optical, dielectric, and $^{13}C$ NMR spectroscopies.[6,7] In the first two methods, the order parameters are obtained from the optical birefringence and from the dielectric anisotropy in the mesophase, respectively. Different anisotropic interactions (i.e., quadrupolar, dipolar, chemical shift) and nuclei can be exploited to investigate orientational order by means of NMR techniques;[8−10] as shown in the previous studies, $^{13}C$ NMR measurements can be successfully applied to F-LCs for determining orientational order parameters from $^{13}C-^{19}F$ couplings or $^{13}C$ chemical shift anisotropies, provided that independent information on molecular geometry and chemical shift tensors is obtained by density functional theory (DFT) calculations.

In the present work, an analogous multidisciplinary approach was applied to two F-LCs belonging to the phenyl-4-(5-alkyl-1,3,2-dioxaborin-2-yl)benzoate homologous series,[4] namely, 5DBF1, showing nematic (N) and smectic A (SmA) phases, and 4DBF2, showing a N phase (Figure 1). In particular, the orientational order of both compounds in their mesophases was analyzed by means of optical and dielectric techniques as in the previous works. In terms of NMR measurements, orientational order parameters for the molecular aromatic core were obtained by exploiting observables from both $^{13}C$ and $^{19}F$ spectra, that is, $^{13}C$ and $^{19}F$ chemical shift anisotropies; $^{13}C-^{19}F$ and, for 5DBF1, $^{19}F-^{1}H$ couplings; and DFT-calculated geometrical parameters and $^{13}C$ and $^{19}F$ chemical shift tensors. Compared to previous works,[6,7] the larger set of experimental data available allowed both a critical analysis of the orientational

* Corresponding authors. M.G.: phone +39-0502219289; fax +39-0502219260; e-mail mg@dcci.unipi.it. L.C.: phone +39-0503152517; fax +39-0503152442; e-mail l.calucci@ipcf.cnr.it.
[†] Università di Pisa.
[‡] Istituto per i Processi Chimico Fisici del CNR.
[§] Jagellonian University.
[||] Military University of Technology.
[⊥] Polish Academy of Sciences.
[#] Scuola Normale Superiore.

10.1021/jp908241n CCC: $40.75 
Published on Web 10/26/2009

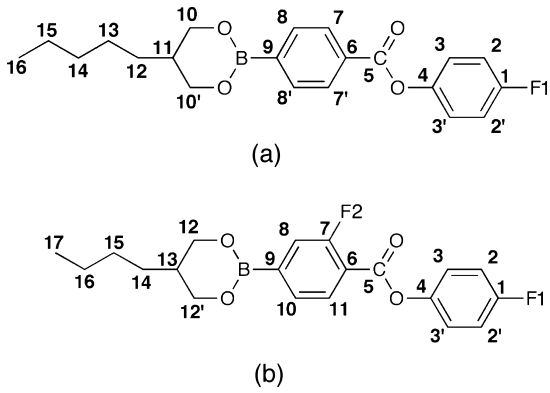


**Figure 1.** Molecular structure and labeling of carbon and fluorine atoms of (a) 5DBF1 and (b) 4DBF2.

order parameters obtained from different subsets of experimental data and their simultaneous use in a global fitting procedure. In particular, the use of the $^{19}$F spectral parameters was tested and discussed in reference to the possible experimental and theoretical sources of error. Moreover, it must be pointed out that advanced DFT methods that include the effects of the environment through a polarizable continuum model (PCM),[11,12] where the liquid-crystalline environment is represented in terms of a tensorial dielectric permittivity, were used for geometry optimizations and $^{13}$C and $^{19}$F chemical-shift-tensor calculations.

## Experimental Methods

**Samples.** The compounds 5DBF1 and 4DBF2 were synthesized following the procedure reported in ref 4. They show enantiotropic mesophases with phase transitions as follows:

5DBF1: Cr—348.4 K—SmA—353.7 K—N—391.1 K—I

4DBF2: Cr—340.4 K—N—358.6 K—I

On cooling, both compounds show at least 30 K of supercooling of the lower-temperature mesophase.

**Optical Measurements.** The optical birefringence, $\Delta n = n_e - n_0$, in the N phase of 4DBF2 and in the N and SmA phases of 5DBF1 was measured by the method described in ref 13. A glass plate and a convex lens comprised a sample cell of variable thickness that was placed between crossed polarizers on a microscopic stage equipped with a heater allowing stabilization of the temperature with an accuracy of ±0.2 K. In this arrangement, a system of circular interference fringes was observed. From the diameters of the fringes, the optical birefringence $\Delta n$ could be calculated. All of the measurements were performed by decreasing the temperature from the isotropic to the liquid-crystalline phases.

**Dielectric Measurements.** The static dielectric permittivity components, $\varepsilon_{\parallel}$ and $\varepsilon_{\perp}$, were measured in the mesophases by means of an impedance analyzer, HP 4192A, using a gold-covered parallel-plate capacitor ($C \approx 50$ pF). The alignment of the samples, with either $\mathbf{E} \parallel \mathbf{B}$ or $\mathbf{E} \perp \mathbf{B}$ ($\mathbf{E}$ being the measuring field), was achieved by a magnetic field $\mathbf{B}$ of 0.8 T. The thickness of the sample was 0.7 mm. The capacitor was filled with the samples by capillary action in the isotropic phase, and then the temperature was decreased step by step to the mesomorphic range. The temperature was stabilized to within ±0.2 K.

**$^{13}$C and $^{19}$F NMR Measurements.** $^{13}$C NMR spectra of 5DBF1 and 4DBF2 in $CDCl_3$ solution were recorded at 298 K on a Bruker AMX300 spectrometer operating at 75.47 MHz for $^{13}$C and at 300.13 MHz for $^{1}$H, equipped with a 5-mm probe; tetramethylsilane (TMS) was used as the internal standard for chemical shift.

Static $^{13}$C direct-excitation (DE) and cross-polarization (CP) NMR spectra on neat 5DBF1 and 4DBF2 were recorded on a double-channel Varian Infinity Plus 400 spectrometer working at 100.56 MHz for $^{13}$C and at 399.89 MHz for $^{1}$H, equipped with a 5-mm goniometric probe. The 90° pulse length was 4.0 and 3.8 $\mu$s for $^{13}$C and $^{1}$H, respectively. A contact time of 5 ms and a linear ramp were used in CP experiments. Decoupling from $^{1}$H nuclei was achieved using the SPINAL-64 sequence[14] with a field of 45 kHz. A recycle delay of 25 s was used, and at least 100 scans were acquired. The chemical-shift scale was set using hexamethylbenzene (HMB) as an external reference and referred to the signal of TMS.

$^{19}$F NMR spectra on neat 5DBF1 and 4DBF2 were recorded on a Varian Unity 300 spectrometer working at 282.23 MHz for $^{19}$F equipped with a 5-mm probe. The $^{19}$F 90° pulse length was 13.8 $\mu$s, and 32 scans were acquired for each spectrum with a recycle delay of 20 s. The chemical shift scale in the mesophases was referred to the chemical shift of $F_1$ in the isotropic phase, assumed to be equal to zero.

For $^{13}$C and $^{19}$F measurements in the mesophases, the samples were uniformly aligned by slow cooling from the isotropic to the nematic phase within the magnetic field. Spectra were recorded on cooling; the temperature was stabilized within ±0.2 K.

**Calculations of Optimized Molecular Geometries and Chemical Shift Tensors.** The molecular structures of 5DBF1 and 4DBF2 were built up by GaussView 3.0 (Gaussian Inc., Pittsburgh, PA), and all of the calculations were performed with the Gaussian 03 computational package.[15] The geometries were optimized with DFT methods at the B3LYP/6-31G(d) level of theory, both in vacuo and simulating the solvent effect using the integral equation formalism of the polarizable continuum model (IEF-PCM).[11] In the last case, the experimental isotropic dielectric permittivity values at 370 K (10.3) and 335 K (14.3) were used for 5DBF1 and 4DBF2, respectively.

The dipole moments, $\mu$, were calculated with MOPAC[16] using the semiempirical AM1 and DFT methods, after optimization of the molecular geometry.

$^{13}$C and $^{19}$F nuclear shielding tensors were determined at the DFT level of theory using the GIAO approach[17,18] with the Perdew—Wang[19] exchange-correlation functional MPW1PW91[20] and the 6-311+G(d,p) basis set, following the recommendations given by Cheeseman et al.[21] Calculations were performed both in vacuo and in the anisotropic environment using the IEF-PCM method.[12] In the latter, the experimental tensor components $\varepsilon_{\parallel}$ and $\varepsilon_{\perp}$ determined at different temperatures in the N phases of the 5DBF1 and 4DBF2 mesogens were used. The chemical shift tensors of $^{13}$C and $^{19}$F were obtained by referring the absolute chemical shielding tensors obtained by DFT to the absolute shieldings of TMS (185.97 ppm) and $CCl_3F$ (188.85 ppm), respectively.

## Results

**Optical Measurements.** A simplified procedure, described in details in refs 13 and 22, was applied to determine the order parameter relative to the principal axis of the polarizability tensor from the optical birefringence $\Delta n = n_e - n_0$, that is, the difference between the extraordinary and ordinary refractive indices. $\Delta n$ was measured throughout the liquid-crystalline ranges of 5DBF1 and 4DBF2; the experimental data obtained

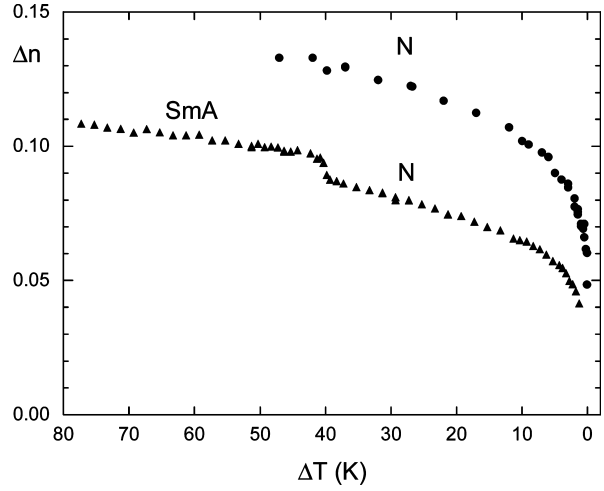


**Figure 2.** Optical birefringence vs shifted temperature in the liquid-crystalline phases of (▲) 5DBF1 and (●) 4DBF2.

are shown in Figure 2 as a function of the shifted temperature $\Delta T = T_{NI} - T$, where $T_{NI}$ is the clearing temperature. The temperature dependence of $\Delta n$ in the N phase was fitted to the form

$$\Delta n = \delta n\left(1 - \frac{T}{T^*}\right)^{\lambda} \quad (1)$$

where $T$ is the absolute temperature and $T^*$, $\delta n$, and $\lambda$ are fitting parameters. This procedure is equivalent to the extrapolation of $\Delta n$ to the temperature of absolute zero. Assuming that, at this temperature, the order parameter is $S = 1$, we can calculate the order parameter as

$$S(T) = \frac{\Delta n(T)}{\delta n} \quad (2)$$

The best-fit parameters were found to be 0.140 and 0.191 ($\delta n$), 394.6 and 359.6 K ($T^*$), and 0.208 and 0.195 ($\lambda$) for 5DBF1 and 4DBF2, respectively. The $\delta n$ value determined for the N phase of 5DBF1 was also used for calculating the order parameter in the SmA phase. The order parameters obtained for both 5DBF1 and 4DBF2 are reported in Figure 3.

**Dielectric Measurements.** The parallel ($\varepsilon_{||}$) and perpendicular ($\varepsilon_{\perp}$) components of the static dielectric permittivity were measured in the isotropic and liquid-crystalline phases of both 5DBF1 and 4DBF2; the obtained values are reported in Figure 4a. In the nematic phase, the dielectric anisotropy, $\Delta\varepsilon = \varepsilon_{||} - \varepsilon_{\perp}$, reported in Figure 4b for both mesogens, can be expressed as a function of the order parameter $S$ relative to the long molecular axis (assumed to be coincident with the minimum-moment-of-inertia axis) according to the Maier and Meier equation[23]

$$\Delta\varepsilon = \frac{N_0 hF}{\varepsilon_0}\left[\Delta\alpha - F\frac{\mu^2}{2k_B T}(1 - 3\cos^2\beta)\right]S \quad (3)$$

where $N_0$ is the number density (which is equal to $N_A\rho/M$, with $N_A$ being Avogadro's number, $\rho$ the density, and $M$ the molar mass), $\varepsilon_0$ is the permittivity of free space, $F$ and $h$ are local field parameters, $k_B$ is the Boltzmann constant, $\Delta\alpha$ is the anisotropy of the molecular polarizability, $\mu$ is the molecular permanent dipolar moment, and $\beta$ is the angle between $\mu$ and the long molecular axis. The local field parameters $F$ and $h$ are dependent on the mean polarizability and the mean dielectric permittivity [$\langle\varepsilon\rangle = (\varepsilon_{||} + 2\varepsilon_{\perp})/3$]. Despite the implied simplifications, eq 3 is commonly used to analyze experimental results.[24−27] For strongly dipolar compounds, the dipolar polarizability $\mu^2/k_B T$ dominates in the square brackets of eq 3, so that $\Delta\alpha$ can be safely neglected; also neglecting the temperature dependence of $N_0$, the following further simplified relation between $\Delta\varepsilon$ and $S$ can thus be applied

$$S(T) \propto \frac{T\Delta\varepsilon(T)}{hF^2} \quad (4)$$

This equation can safely be used to analyze the dielectric permittivity anisotropy of 5DBF1 and 4DBF2, for which the relationship $\Delta\alpha \ll F\mu^2/2k_B T$ holds. In fact, on the basis of the birefringence values, we can assume $\Delta\alpha \approx 10$ Å$^3$, while the dipole moment values determined by means of semiempirical and DFT methods are, respectively, 5.73 and 6.49 D for 5DBF1 and 6.49 and 7.49 D for 4DBF2, and the values of the local field parameter $F$ range from 1.51 to 1.55 for 5DBF1 and from 1.51 to 1.59 for 4DBF2. Moreover, the local field parameter $h$ ranges from 1.38 to 1.44 for 5DBF1 and from 1.42 to 1.47 for 4DBF2. Because the absolute value of the order parameter cannot be determined directly using eq 4, the Haller equation[28]

$$S(T) = S_0(\Delta T)^{\gamma} \quad (5)$$

was assumed to describe the trend of $S$ with the shifted temperature, with $S_0 = 1/T_{NI}^{\gamma}$.[29] Combining eqs 4 and 5, the order-parameter values reported in Figure 3 were determined for 5DBF1 and 4DBF2 with best-fit $\gamma$ values of 0.122 and 0.167, respectively.

**$^{13}$C and $^{19}$F NMR Spectroscopy.** ***Assignment of Spectra and Determination of Spectral Parameters.*** $^{13}$C DE NMR spectra under proton decoupling were recorded in the isotropic phase of both mesogens; as shown in Figure 5, 16 and 17 signals, corresponding to chemically nonequivalent carbons, could be resolved in the spectra of 5DBF1 and 4DBF2, respectively. Very similar $^{13}$C NMR spectra were obtained in $CDCl_3$ solution (not shown), but with narrower lines, allowing for the determination of smaller $^{13}$C−$^{19}$F scalar coupling constants ($J^{iso}$). The assignments and the chemical shift values of the signals in both the isotropic phase and $CDCl_3$ solution are reported in Table 1, together with the chemical shift values calculated using the GIAO−DFT method; as can be observed, the agreement between the experimental and calculated data is quite good. The values of $J^{iso}$ determined for the different carbons in $CDCl_3$ solution are reported in Tables 2 and 3 for 5DBF1 and 4DBF2, respectively.

$^{13}$C CP NMR spectra under proton decoupling were recorded at different temperatures in the mesophases of both 5DBF1 and 4DBF2 uniformly aligned with the phase director parallel to the magnetic field; expansions of the aromatic regions of representative spectra are shown in Figure 6. As can be seen, the interpretation of the spectra is more difficult than for the isotropic phase because of the presence of the anisotropic components of the chemical shift ($\delta^{aniso}$) and $^{13}$C−$^{19}$F dipolar and scalar ($J$) interactions. In particular, the dipolar and $J$ couplings split each $^{13}$C aromatic signal into one doublet for each $^{19}$F nucleus present in the ring, with splittings ranging from tens to thousands of hertz, essentially depending on the distance

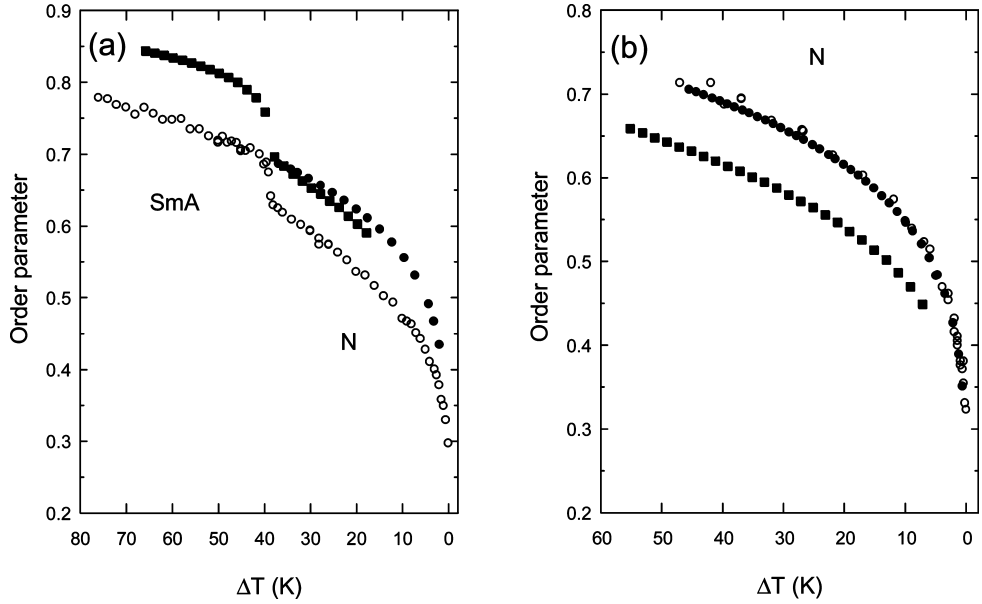


**Figure 3.** Order parameter vs shifted temperature for (a) 5DBF1 and (b) 4DBF2 determined from (■) NMR, (○) optical, and (●) dielectric spectroscopies as explained in the text.

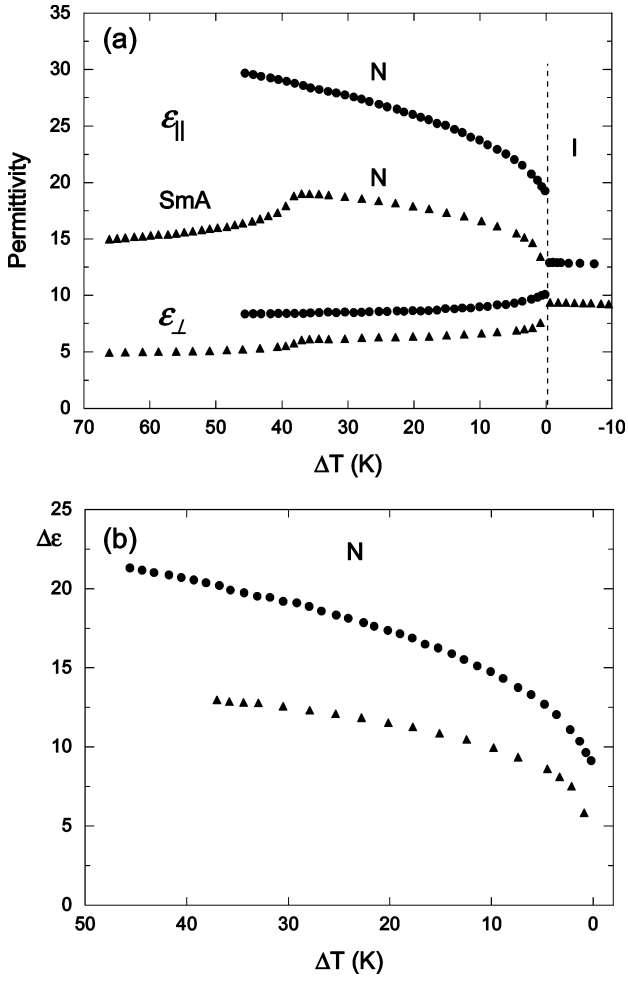


**Figure 4.** (a) Static dielectric permittivity components and (b) dielectric anisotropy vs shifted temperature for (▲) 5DBF1 and (●) 4DBF2.

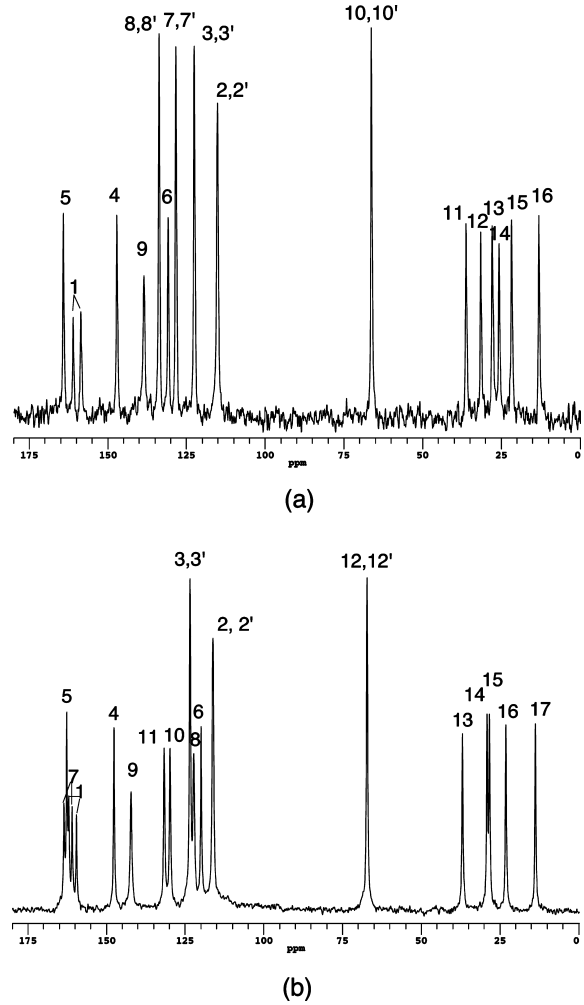


**Figure 5.** $^{13}$C DE NMR spectra under proton decoupling of (a) 5DBF1 and (b) 4DBF2 in the isotropic phase with spectral assignment.

between the $^{13}$C and $^{19}$F nuclei and the direction of the internuclear vector with respect to the magnetic field. On the other hand, chemical shift anisotropy gives rise to a high-frequency shift of the center of the multiplets by up to 80 ppm. It should be noticed that small splittings due to $^{13}$C−$^{19}$F dipolar couplings between carbons of ring A and F2 were also observed in the $^{13}$C spectra of 4DBF2. The achieved spectral resolution allowed the resonances of all of the carbons in the aromatic

**TABLE 1: $^{13}C$ Isotropic Chemical Shifts (ppm) of 5DBF1 and 4DBF2 Measured from Spectra in the Melt Isotropic Phase ($\delta_{Melt}$) and in $CDCl_3$ Solution ($\delta_{CDCl_3}$) and Calculated by the GIAO−DFT Method in Vacuo ($\delta_{GIAO}$)**

| 5DBF1 | | | | 4DBF2 | | | |
|---|---|---|---|---|---|---|---|
| C*n* | $\delta_{GIAO}$ | $\delta_{CDCl_3}$ | $\delta_{Melt}$ | C*n* | $\delta_{GIAO}$ | $\delta_{CDCl3}$ | $\delta_{Melt}$ |
| 1 | 161.9 | 159.9 | 160.0 | 1 | 161.9 | 160.5 | 160.8 |
| 2,2′ | 115.2 | 116.2 | 115.3 | 2,2′ | 115.1 | 116.2 | 116.4 |
| 3,3′ | 123.1 | 123.3 | 122.7 | 3,3′ | 123.1 | 123.3 | 123.6 |
| 4 | 148.4 | 146.9 | 147.2 | 4 | 148.2 | 146.6 | 147.7 |
| 5 | 164.4 | 165.6 | 164.2 | 5 | 161.6 | 163.1 | 162.7 |
| 6 | 131.3 | 130.9 | 131.0 | 6 | 118.6 | 119.2 | 120.1 |
| 7,7′ | 129.6 | 129.2 | 128.5 | 7 | 165.7 | 162.0 | 162.3 |
| 8,8′ | 134.5 | 134.0 | 133.9 | 8 | 123.0 | 122.1 | 122.4 |
| 9 | 138.1 | 138.8 | 138.6 | 9 | 141.2 | 141.8 | 142.3 |
| 10,10′ | 63.9 | 67.1 | 66.5 | 10 | 129.0 | 129.2 | 129.9 |
| 11 | 34.5 | 36.6 | 36.5 | 11 | 132.5 | 131.6 | 131.8 |
| 12 | 30.8 | 32.0 | 31.8 | 12,12′ | 64.7 | 67.1 | 67.4 |
| 13 | 27.3 | 28.3 | 28.1 | 13 | 35.4 | 36.5 | 37.1 |
| 14 | 26.1 | 26.6 | 26.0 | 14 | 28.2 | 29.0 | 29.3 |
| 15 | 21.6 | 22.6 | 22.0 | 15 | 28.1 | 28.0 | 28.5 |
| 16 | 10.5 | 14.1 | 13.3 | 16 | 22.0 | 22.9 | 23.4 |
| | | | | 17 | 12.4 | 14.0 | 14.0 |

**TABLE 2: Geometrical ($r_{1n}$ and $\theta_{zn}$) and NMR ($J^{iso}$, $\Delta J$, $J_{xx} - J_{yy}$, and $D^h$) Parameters Relative to the Fluorinated Aromatic Ring of 5DBF1 Used in the Analysis of the $^{13}C-^{19}F$ Couplings**

| C*n* | $r_{1n}$[a] (Å) | $\theta_{zn}$[b] (deg) | $J^{iso}$ (Hz) | $\Delta J$ (Hz) | $J_{xx} - J_{yy}$ (Hz) | $D^h$ (%) |
|---|---|---|---|---|---|---|
| 1 | 1.351 | 0.00 | −244.1 | 400.0 | 13.0 | −2.57 |
| 2,2′ | 2.362 | ±30.90 | 23.7 | −39.0 | −20.5 | −0.99 |
| 3,3′ | 3.651 | ±19.45 | 8.5 | 17.6 | 13.7 | −0.35 |
| 4 | 4.106 | 0.00 | 2.8 | | | −0.14 |

[a] Distance between F1 and C*n*. [b] Angle between the F1−C*n* vector and the *z* axis of the frame located on the phenyl ring.

core to be assigned in the case of 5DBF1 (Figure 6, left), whereas only the signals due to carbons C1, C2, C2′, C3, C3′, C4, C5, C6, and C7 were unambiguously assigned in that of 4DBF2 (Figure 6, right). It should also be pointed out that fast phenyl ring flips render equivalent the pairs of carbons C2/C2′ and C3/C3′ on ring A of both mesogens, as well as the pairs C7/C7′ and C8/C8′ on ring B of 5DBF1. The large line width observed for C9 in the spectra of 5DBF1 can be ascribed to bonding to boron quadrupolar nuclei, either $^{10}B$ or $^{11}B$, affecting the $^{13}C$ line shape through both indirect and dipole couplings and relaxation effects.[30] The assignment of the spectra was performed on the basis of the magnitudes of both chemical shift anisotropies and $^{13}C-^{19}F$ couplings,[6] as well as the trends of signals with temperature (Figure 6). The values of the chemical shift anisotropies ($\delta^{aniso}$) were obtained at each temperature by subtracting the isotropic value measured in the melt isotropic phase ($\delta^{iso}$) from the chemical shift value measured in the mesophase ($\delta^{obs}$)

$$\delta^{obs} = \delta^{iso} + \delta^{aniso} \quad (6)$$

Moreover, the $^{13}C-^{19}F$ splitting ($\Delta_{ij}$), that is, the separation between the two lines of the doublet due to coupling between a $^{13}C$ nucleus *i* and an $^{19}F$ nucleus *j*, was determined from the spectral analysis for each C*i*−F*j* pair. These values are given by contributions from both dipolar and scalar interactions

$$\Delta_{ij} = 2D_{ij}^{exp} + J_{ij}^{iso} \quad (7)$$

where $J_{ij}^{iso}$ is the scalar spin−spin coupling between the two nuclei, here taken from measurements in $CDCl_3$ solution (see Tables 2 and 3), and $D_{ij}^{exp}$ results from the combination of the dipolar coupling and the anisotropic contribution to the spin−spin coupling. The obtained values of $\delta^{aniso}$ and $D_{ij}^{exp}$ are reported in Figures 7 and 8 for 5DBF1 and 4DBF2, respectively.

$^{19}F$ NMR spectra were also recorded in the isotropic and mesomorphic phases of both 5DBF1 and 4DBF2; representative spectra are shown in Figure 9. In the case of 5DBF1, a single sharp line was observed in the isotropic phase, whereas a broad peak was present at all temperatures in the mesophases; moreover, a sudden low-frequency shift was observed upon entering the nematic and SmA phases, and the chemical shift progressively decreased with decreasing temperature within both mesophases. For 4DBF2 two sharp lines, ascribable to F1 and F2, were detected in the isotropic phase, whereas a broad line, analogous to that found for 5DBF1, and a doublet of broad lines were observed in the nematic phase. The single line, which was shifted to low frequency with respect to the corresponding isotropic line, was ascribed to F1, whereas the doublet, whose center of mass was high-frequency-shifted, was assigned to F2. As the temperature was decreased within the nematic phase, the chemical shift of F1 regularly decreased, whereas both the chemical shift and the splitting of the F2 doublet increased. The $^{19}F$ NMR spectral features can be explained on the basis of the anisotropies of both the fluorine chemical shift and the $^{1}H-^{19}F$ dipolar couplings; the different multiplicities of the F1 and F2 signals are essentially due to the different orientations of the $^{1}H-^{19}F$ internuclear vectors between fluorine and the closest proton(s) with respect to the magnetic field, which are expected to be almost parallel for F2 and close to the magic angle for F1. On the other hand, the different signs of the shifts of the two signals with temperature are due to the different $^{19}F$ chemical shift tensor components and orientations. The trends of $\delta^{aniso}$ and $D_{ij}^{exp}$ obtained from the spectral analysis according to eqs 6 and 7 are reported in Figures 7 and 8 for 5DBF1 and 4DBF2, respectively.

***Determination of Order Parameters.*** Orientational order parameters of the rigid aromatic fragments of 4DBF2 and 5DBF1 were determined through a global-fitting procedure using a very large set of experimental NMR data: $^{13}C$ and $^{19}F$ $\delta^{aniso}$ values and $^{13}C-^{19}F$ and $^{1}H-^{19}F$ $D_{ij}^{exp}$ values for the nuclei belonging to the two aromatic rings. The use of further NMR data available from $^{13}C$ spectra, such as $^{13}C$ chemical shift anisotropies for aliphatic nuclei or $^{13}C-^{19}F$ couplings between nuclei belonging to different aromatic rings, would require the application of more sophisticated models involving the conformational analysis of either the aromatic fragment or the aliphatic chains and was beyond the scope of this work. On the other hand, to investigate the reliability of the different experimental and theoretical parameters and their effects on the determined orientational order parameters, we applied the fitting procedure to different subsets of data (chemical shift anisotropies, dipolar couplings, data from $^{13}C$ nuclei only, data from single aromatic rings, etc.). In particular, local orientational order parameters relative to the single aromatic rings and to the whole aromatic core of the two mesogens were determined; in the latter case, the fragment including the two aromatic rings and the carboxyl group was considered planar and rigid except for rapid $\pi$-flips of the rings. Also, considering the $D_{\infty h}$ symmetry of N and SmA phases, two independent order parameters, $S_{zz}$ and $S_{xx} - S_{yy}$, with (*x*, *y*, *z*) being the principal axis set for which the Saupe order matrix is diagonal, describe the order of either the aromatic core, phenyl ring A of

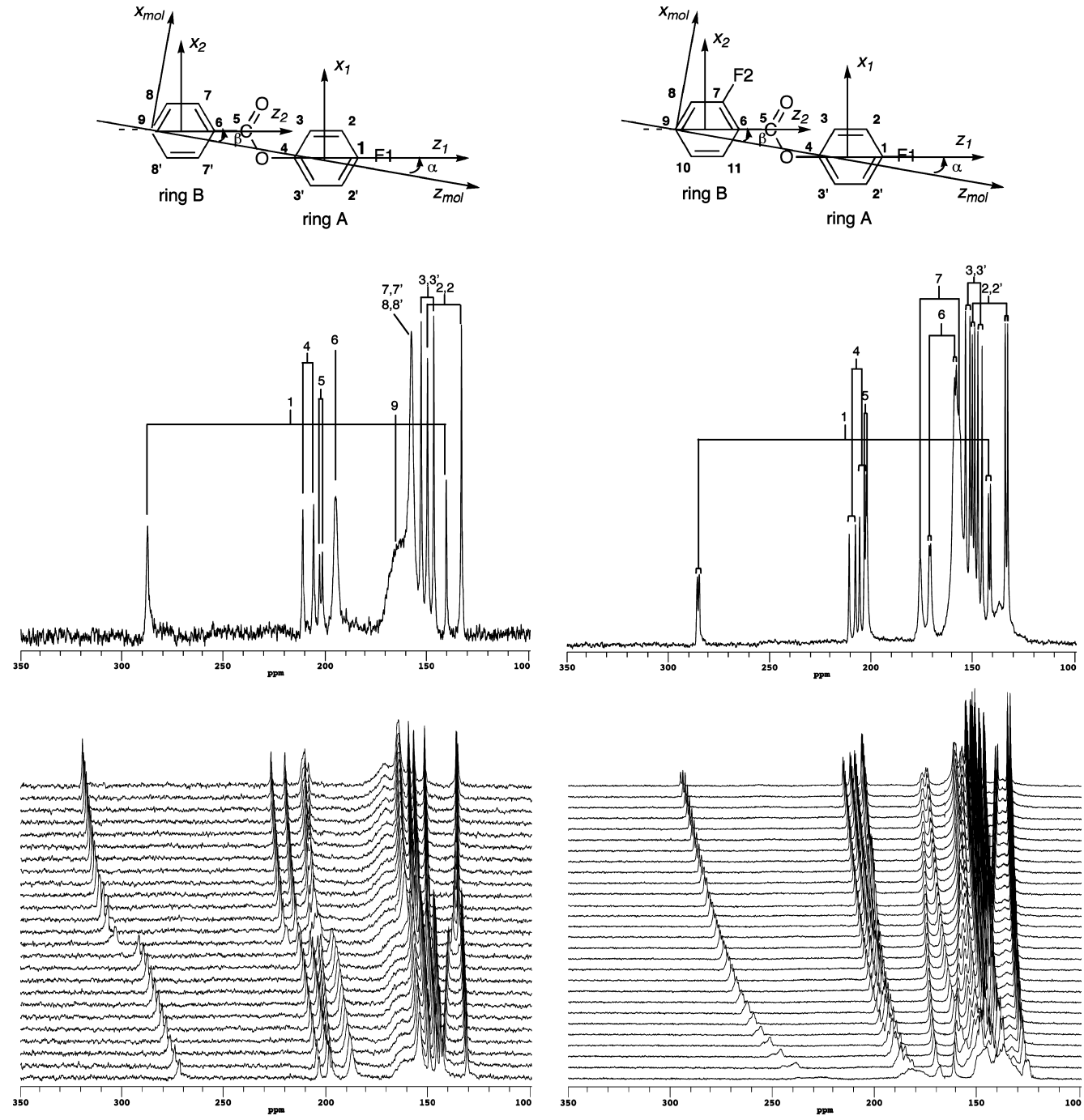


**Figure 6.** Left side: Structure of the aromatic core of 5DBF1 with carbon labeling and axis systems used in the orientational order analysis, aromatic region of the $^{13}C$ NMR CP spectrum of 5DBF1 in the N phase at 357 K with signal assignments, and evolution of the aromatic spectral region with temperature (325−373 K, from top to bottom) in the N and SmA phases. Right side: Structure of the aromatic core of 4DBF2 with carbon numbering and axis systems used in the orientational order analysis, aromatic region of the $^{13}C$ NMR CP spectrum of 4DBF2 in the N phase at 319 K with signal assignments, and evolution of the aromatic spectral region with temperature (303−357 K, from top to bottom) in the N phase.

both mesogens, or ring B of 5DBF1, whereas a third order parameter ($S_{xz}$) has to be used for ring B of 4DBF2.

For each carbon or fluorine nucleus $i$, $\delta^{aniso}$ can be expressed in terms of local order parameters relative to frames on the phenyl rings as

$$\delta_i^{aniso} = \frac{2}{3}\left[\Delta\delta_i S_{zz} + \frac{1}{2}(\delta_{i,xx} - \delta_{i,yy})(S_{xx} - S_{yy}) + 2\delta_{i,xz}S_{xz}\right] \quad (8)$$

where $S_{xz} \neq 0$ only for ring B of 4DBF2 and

$$\Delta\delta_i = \delta_{i,zz} - \frac{1}{2}(\delta_{i,xx} + \delta_{i,yy}) \quad (9)$$

For each couple $i,j$ of $^{19}F$ and $^{13}C$ or $^{1}H$ nuclei, $D_{ij}^{exp}$ results from the sum

$$D_{ij}^{exp} = D_{ij}^{eq} + D_{ij}^{h} + D_{ij}^{ah} + D_{ij}^{d} + \frac{1}{2}J_{ij}^{aniso} \qquad (10)$$

where $D_{ij}^{eq}$ is the dipolar coupling corresponding to the equilibrium structure of the molecule; $D_{ij}^{h}$ and $D_{ij}^{ah}$ are the contribution from the harmonic and anharmonic vibrations, respectively; and $D_{ij}^{d}$ is the contribution arising from the deformation of the molecular structure induced by the anisotropic forces of the medium surrounding the molecules.[31] The terms $D_{ij}^{ah}$ and $D_{ij}^{d}$ are usually very small,[32] so that, considering the error in the measured splittings, they could be safely neglected in the cases investigated here. On the other hand, the term $D_{ij}^{h}$, which depends on the distance between the coupled nuclei $r_{ij}$ as $1/r_{ij}^{5}$,[33] was considered a non-negligible correction of $D_{ij}^{eq}$ only for couples of nuclei that were spatially close; a rough estimation of this contribution could be obtained from the values determined for molecules with similar structure and orientation properties.[30] The term $D_{ij}^{eq}$ can be expressed in terms of the local order parameter $S_{ij}$ relative to the internuclear $ij$ direction and the equilibrium internuclear distance $r_{ij}$ as

$$D_{ij}^{eq} = -\frac{\mu_0 \hbar \gamma_i \gamma_j S_{ij}}{8\pi^2 r_{ij}^{3}} \qquad (11)$$

$J_{ij}^{aniso}$ can be written in terms of local order parameters relative to a phenyl ring as

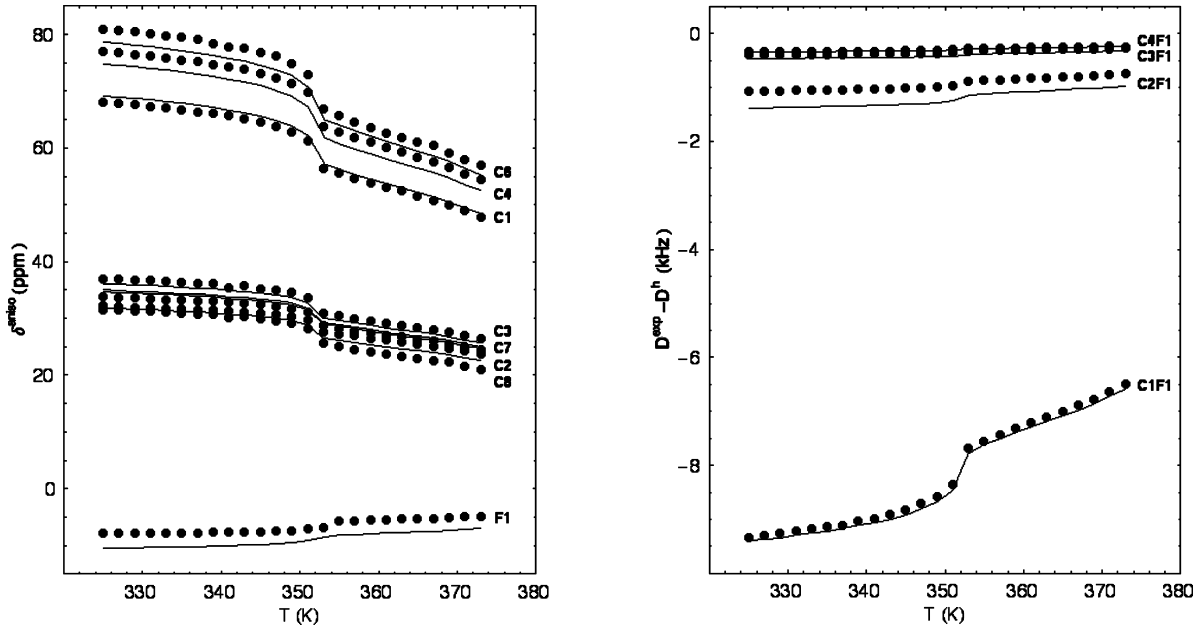


**Figure 7.** Experimental (circles) and calculated (lines) values of (left) $\delta^{aniso}$ for the indicated $^{13}C$ and $^{19}F$ nuclei and (right) $D^{exp} - D^{h}$ for the indicated $^{13}C-^{19}F$ pairs of 5DBF1 as a function of temperature. The data refer to the simultaneous fitting of all experimental data for rings A and B, as described in the text.

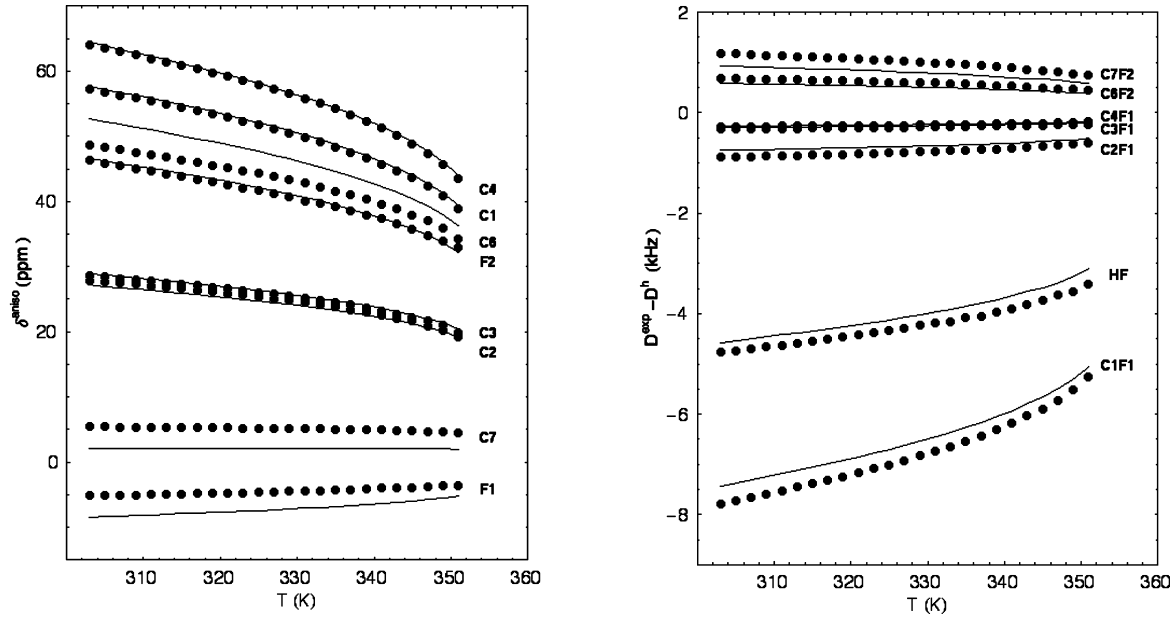


**Figure 8.** Experimental (circles) and calculated (lines) values of (left) $\delta^{aniso}$ for the indicated $^{13}C$ and $^{19}F$ nuclei and (right) $D^{exp} - D^{h}$ for the indicated $^{13}C-^{19}F$ and $^{1}H-^{19}F$ pairs of 4DBF2 as a function of temperature. The data refer to the simultaneous fitting of all experimental data for rings A and B, as described in the text.

$$J_{ij}^{\text{aniso}} = \frac{2}{3}\left[\Delta J_{ij} S_{zz} + \frac{1}{2}(J_{ij,xx} - J_{ij,yy})(S_{xx} - S_{yy}) + 2J_{ij,xz} S_{xz}\right] \quad (12)$$

where $S_{xz} \neq 0$ only for ring B of 4DBF2 and

$$\Delta J_{ij} = J_{ij,zz} - \frac{1}{2}(J_{ij,xx} + J_{ij,yy}) \quad (13)$$

The local order parameters can, in turn, be expressed in terms of the elements of the Saupe order matrix relative to a frame fixed on a rigid molecular fragment using the relationship

$$S_{ij} = \sum_{\alpha,\beta} l_{i\alpha} S_{\alpha\beta} l_{\beta j} \quad (14)$$

where $l_{i\alpha}$ is the direction cosine between the $i$ and $\alpha$ axes.

Following the literature,[30,31] the contribution of $J_{ij}^{\text{aniso}}$ to $D_{ij}^{\text{exp}}$ was considered significant for $^{13}C-^{19}F$ couplings, but neglected for the $^{19}F-^{1}H$ coupling. Considering that the principal order axis of each mesogen presumably lies close to the long molecular axis and taking into account the molecular geometry, the signs of the $D_{ij}^{\text{exp}}$ couplings were assigned to the different couples of nuclei as shown in Figures 7 and 8. The geometrical parameters (i.e., bond lengths and angles, internuclear distances, angles for reference frame transformations) and chemical shift tensor components and orientations used in the determination of order parameters were obtained from DFT calculations performed taking into account the liquid-crystalline medium by using the IEF-PCM method;[11,12] their values are reported in Tables 2−5, except for the data relative to the $^{19}F-^{1}H$ coupling, for which the internuclear vector was parallel to the ring para axis and the internuclear distance was found to be 2.535 Å. For 4DBF2, calculations were performed for the two minimum-energy conformations corresponding to values of the O−C5−C6−C7 dihedral angle of 0° and 180°. The values of the **J** tensor components and the contribution percentage of $D^{\text{h}}$ to $D^{\text{exp}}$ used in the order parameter determinations were estimated from data reported in refs 30 and 31, respectively; they are included in Tables 2 and 3.

In the case of 5DBF1, we could exploit seven $^{13}C$ chemical shift anisotropies, four relative to ring A and three relative to ring B, and four $^{13}C-^{19}F$ $D_{ij}^{\text{exp}}$ couplings for carbons of ring A,

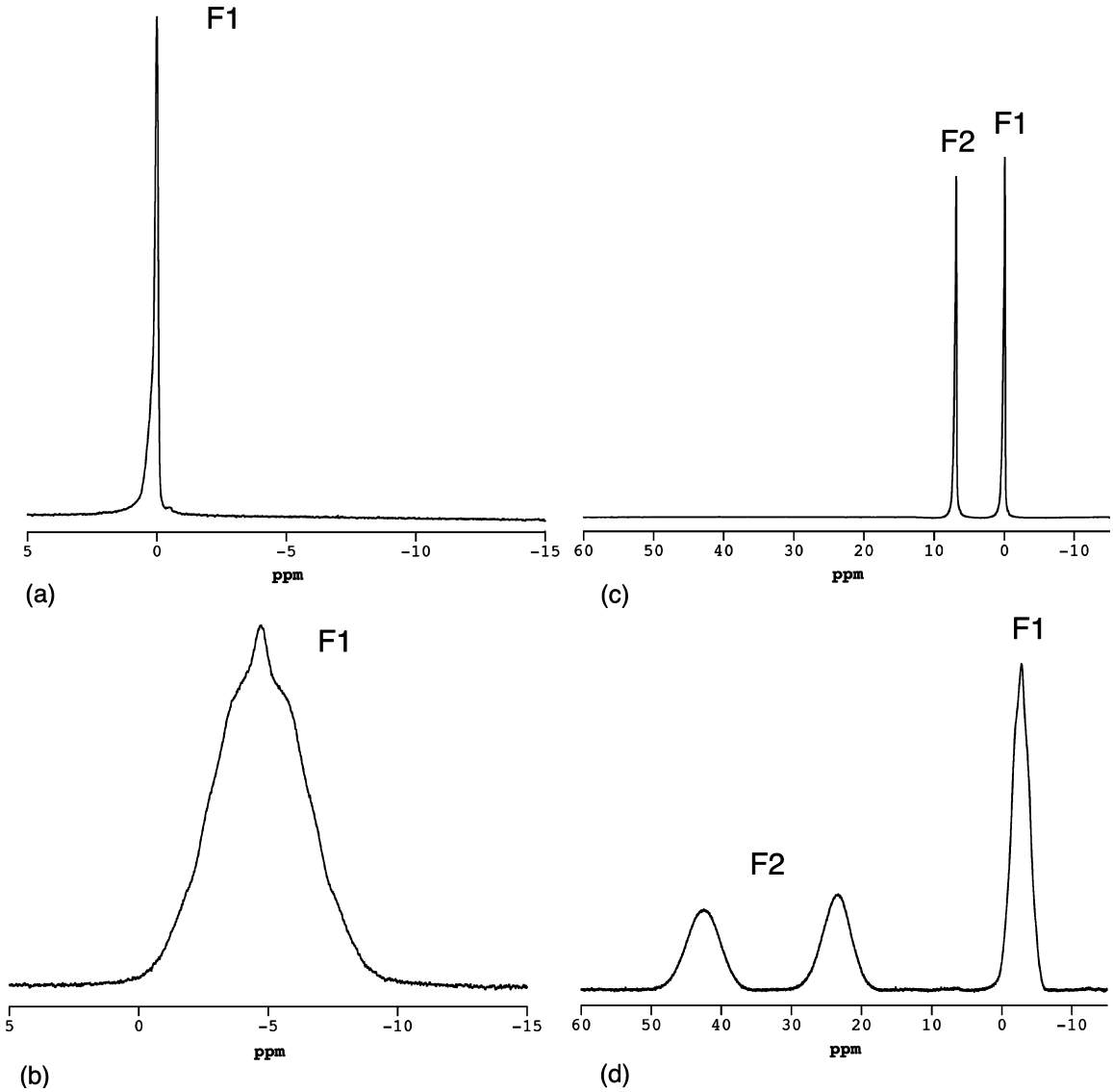


**Figure 9.** $^{19}F$ NMR spectra of 5DBF1 (a) in the isotropic phase at 403 K and (b) in the nematic phase at 373 K, and of 4DBF2 (c) in the isotropic phase at 363 K and (d) in the nematic phase at 355 K.

**TABLE 3: Geometrical ($r_{in}$ and $\theta_{zn}$) and NMR ($J^{iso}$, $\Delta J$, $J_{xx} - J_{yy}$, $J_{xz}$, and $D^h$) Parameters Relative to the Fluorinated Aromatic Rings of 4DBF2 Used in the Analysis of the $^{13}C-^{19}F$ Couplings**

| F*i* | C*n* | $r_{in}$[a] (Å) | $\theta_{zn}$[b] (deg) | $J^{iso}$ (Hz) | $\Delta J$ (Hz) | $J_{xx} - J_{yy}$ (Hz) | $J_{xz}$ (Hz) | $D^h$ (%) |
|---|---|---|---|---|---|---|---|---|
| 1 | 1 | 1.353 | 0.00 | −244.1 | 400.0 | 13.0 | | −2.57 |
| 1 | 2,2′ | 2.362 | ±31.04 | 23.5 | −39.0 | −20.5 | | −0.99 |
| 1 | 3,3′ | 3.631 | ±19.45 | 8.5 | 17.6 | 13.7 | | −0.35 |
| 1 | 4 | 4.103 | 0.00 | 2.8 | | | | −0.14 |
| 2 | 6 | 2.394 | 87.16 | 9.6 | | | | −0.99 |
| 2 | 7 | 1.346 | 57.70 | −261.7 | −63.6 | 322.0 | 161.6 | −2.57 |

[a] Distance between F*i* and C*n*. [b] Angle between the F*i*−C*n* vector and the *z* axis of the frame located on the phenyl ring to which the nuclei belong.

**TABLE 4: Calculated (GIAO−DFT) Chemical-Shift-Tensor (CST) Components $\delta_{ii}$ (ppm) and Angle $\gamma$ (deg) between the *z* Axis of the CST Principal Axes System (PAS) and the Phenyl-Ring Para Axis Obtained for the Minimum-Energy Conformer of 5DBF1 via the IEF-PCM Method Using Experimental Dielectric Permittivity Components at 355 K, As Explained in Experimental Methods**

| C*n* | $\delta_{zz}$ | $\delta_{xx}$ | $\delta_{yy}$ | $\gamma$ |
|---|---|---|---|---|
| 1 | 247.8 | 142.3 | 96.3 | 3.5 |
| 2 | 198.9 | 135.6 | 12.4 | 58.0 |
| 3 | 212.8 | 151.1 | 9.9 | 123.6 |
| 4 | 241.6 | 131.9 | 71.7 | 4.4 |
| 3′ | 211.0 | 140.1 | 15.4 | −125.4 |
| 2′ | 200.8 | 135.5 | 12.2 | −58.1 |
| 5 | 262.4 | 120.0 | 116.0 | −36.2 |
| 6 | 225.0 | 143.7 | 24.1 | −0.7 |
| 7 | 240.6 | 151.0 | 0.6 | 61.6 |
| 8 | 248.7 | 152.5 | 2.3 | 119.6 |
| 9 | 237.2 | 189.3 | −8.0 | 0.0 |
| 8′ | 248.9 | 151.7 | 2.9 | −119.9 |
| 7′ | 231.5 | 152.7 | 2.5 | −60.7 |
| F1 | −129.8 | −37.9 | −178.4 | 2.4 |

**TABLE 5: Calculated (GIAO−DFT) CST Components $\delta_{ii}$ (ppm) and Angle $\gamma$ (deg) between the *z* Axis of the CST PAS and the Phenyl-Ring Para Axis Obtained for the Two Most Populated Conformers of 4DBF2 via the IEF-PCM Method Using Experimental Dielectric Permittivity Components at 358 K, As Explained in Experimental Methods**

| | conformer 1 | | | | conformer 2 | | | |
|---|---|---|---|---|---|---|---|---|
| C*n* | $\delta_{zz}$ | $\delta_{xx}$ | $\delta_{yy}$ | $\gamma$ | $\delta_{zz}$ | $\delta_{xx}$ | $\delta_{yy}$ | $\gamma$ |
| 1 | 249.3 | 143.1 | 97.8 | 4.0 | 249.1 | 143.0 | 97.8 | 6.3 |
| 2 | 200.1 | 136.9 | 12.7 | 62.4 | 200.4 | 136.9 | 12.8 | 60.3 |
| 3 | 216.8 | 146.6 | 14.0 | 119.8 | 216.4 | 145.9 | 14.0 | 118.6 |
| 4 | 244.5 | 127.8 | 73.7 | 2.4 | 244.5 | 127.1 | 74.2 | 1.4 |
| 3′ | 215.2 | 141.5 | 15.0 | −120.0 | 214.5 | 141.7 | 14.9 | −119.8 |
| 2′ | 201.3 | 136.7 | 12.6 | −59.9 | 201.4 | 137.0 | 12.6 | −62.0 |
| 5 | 258.8 | 121.7 | 114.9 | −34.3 | 262.6 | 117.4 | 111.7 | 35.2 |
| 6 | 183.9 | 140.7 | 26.6 | −3.1 | 184.4 | 141.7 | 27.4 | −0.3 |
| 7 | 250.4 | 149.8 | 98.9 | 65.4 | 242.3 | 153.9 | 98.4 | 64.4 |
| 8 | 213.4 | 140.0 | 14.7 | 117.0 | 213.5 | 139.7 | 15.1 | 117.2 |
| 9 | 236.7 | 195.4 | −0.8 | 0.2 | 236.6 | 194.4 | 0.2 | 0.0 |
| 10 | 242.0 | 146.3 | 1.8 | −119.4 | 241.6 | 147.1 | 1.5 | −119.7 |
| 11 | 231.4 | 155.9 | 9.2 | −62.9 | 240.3 | 153.8 | 8.4 | −64.0 |
| F1 | −130.2 | −34.8 | −171.6 | 4.6 | −129.5 | −34.9 | −172.1 | 5.1 |
| F2 | −83.4 | −16.7 | −190.6 | 64.7 | −85.3 | −10.6 | −204.5 | 65.2 |

as well as the chemical shift anisotropy of the sole $^{19}F$ nucleus present. When the data for the sole A ring were taken into account to obtain order parameters relative to the local axis system ($x_1$, $y_1$, $z_1$), the $^{13}C$ $\delta^{aniso}$ and $^{13}C-^{19}F$ $D_{ij}^{exp}$ values were in very good agreement, and substantially identical orientational order parameters were obtained using these two independent sets of data (see Figure 10a). By using $^{13}C$ $\delta^{aniso}$ and $^{13}C-^{19}F$ $D_{ij}^{exp}$ values for ring A together in the fitting, the maximum deviations obtained between the experimental and calculated data were very small (1.5 ppm for chemical shifts and 25 Hz for $D_{ij}^{exp}$); the local order parameter $S_{zz}$ so obtained for ring A ranged from 0.571 to 0.818 throughout the temperature range investigated (from 373 to 325 K), whereas the biaxiality ($S_{xx} - S_{yy}$) was less than 0.015 in both the N and SmA phases. The introduction of the $^{19}F$ chemical shift anisotropy induced a marked increase of the deviations, which, however, were still acceptably low (up to 3 ppm for chemical shifts and 100 Hz for $D_{ij}^{exp}$), whereas the order parameters did not change much ($S_{zz}$ ranged from 0.566 to 0.810, and biaxiality was lower than 0.03). Because only three $^{13}C$ chemical shift anisotropies were available for ring B (i.e., those relative to carbons C6, C7/C7′, and C8/C8′), the same analysis made for ring A could not be performed. Therefore, we analyzed together data from rings A and B to obtain molecular order parameters referred to the ($x_{mol}$, $y_{mol}$, $z_{mol}$) axis frame, whose position was not known and was to have been determined by finding the angles $\alpha$ and $\beta$ between the $z_{mol}$ axis and the para axes of rings A and B, respectively, as best-fitting parameters. We performed some preliminary test to see which angles gave the best reproduction of the experimental data. We observed that the best value for the angle between the two para axes of rings A and B was always very similar to the value of 11° obtained by DFT geometry optimization, so we decided to keep this value fixed to reduce the correlation among fitting parameters. By comparing the fitting results obtained using data from the two rings with the corresponding results for ring A only, we observed an increase of the deviations between the experimental and calculated data (maximum deviations of 4 ppm for chemical shifts and 300 Hz for $D_{ij}^{exp}$). The orientational order parameters obtained when all of the experimental data were used in a global fitting were $S_{zz}$ ranging from 0.591 to 0.844 (see Figure 3) and biaxiality ranging between −0.01 and 0.00; in addition, the $z_{mol}$ axis was found to form angles of $\alpha = -7°$ and $\beta = 4°$ with the para axes of the rings. Molecular biaxiality was substantially null in the whole mesomorphic range, as expected on the basis of the cylindrical symmetry of the molecule. The trend of $S_{zz}$ exhibited a jump between 351 and 353 K, indicating a first-order character for the $N-S_A$ phase transition, in agreement with optical birefringence findings.

In 4DBF2, the presence of two fluorine atoms, one each in rings A and B, complicated the spectral interpretation, as previously discussed, but at the same time, it allowed a higher number of experimental data points to be available. In fact, for this mesogen, six $^{13}C$ chemical shift anisotropies and the same number of $^{13}C-^{19}F$ $D_{ij}^{exp}$ couplings, four relative to ring A and two relative to ring B (i.e., those of carbons C6 and C7), could be exploited, as well as one $^{19}F$ chemical shift anisotropy for each ring and the $^{1}H-^{19}F$ coupling between F2 and the proton bound to C8 in ring B. Therefore, in this case, we could determine individual local orientational order parameters for ring A [relative to the ($x_1$, $y_1$, $z_1$) axis system] and for ring B [relative to the ($x_2$, $y_2$, $z_2$) axis system]. Those obtained for ring A were scarcely affected by the set of data used in the fitting. For instance, using $^{13}C-^{19}F$ couplings only, $^{13}C$ chemical shift anisotropies only, or the whole set of data available, the maximum variation of $S_{zz}$ was by 4%; in Figure 10b, the local order parameters obtained considering $^{13}C-^{19}F$ couplings only and $^{13}C$ chemical shift anisotropies only are compared. The maximum errors were 1 and 2.2 ppm for $^{13}C$ and $^{19}F$ chemical shifts, respectively, and 200 Hz for $D_{ij}^{exp}$. On the contrary, the results for ring B appear to be much less reliable, more strongly

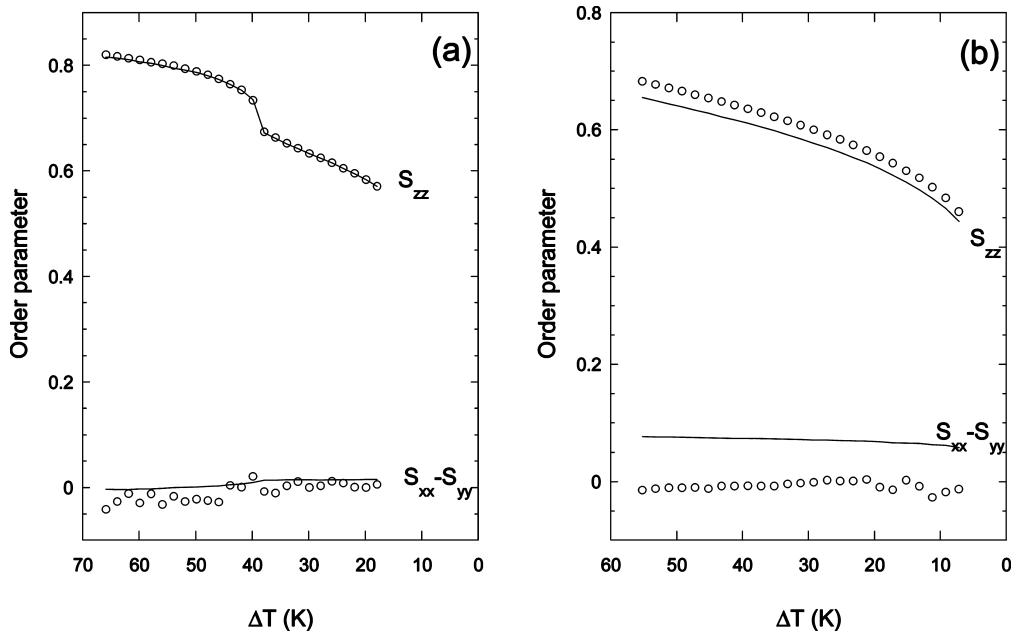


**Figure 10.** Local order parameters relative to ring A vs shifted temperature for (a) 5DBF1 and (b) 4DBF2 obtained from the analysis of $^{13}C$ chemical shift anisotropies (lines) or $^{13}C-^{19}F$ couplings (circles).

depending on the experimental data used in the fitting. For example, $S_{zz}$ varied by 8% when the $^{19}F$ chemical shift anisotropy and $^{1}H-^{19}F$ coupling were added to the $^{13}C$ data in the fitting, with a marked increase in the deviations between the experimental and calculated data, particularly for chemical shifts (from 0.3 to 4.5 ppm); on the other hand, the maximum errors in $D_{ij}^{exp}$ were less than 60 and 350 Hz for $^{13}C-^{19}F$ and $^{1}H-^{19}F$ couplings, respectively. When data from both rings of 4DBF2 were put together in the fitting, as in the case of 5DBF1, to obtain orientational order parameters for the aromatic core relative to the ($x_{mol}$, $y_{mol}$, $z_{mol}$) axis system, preliminary tests indicated that the angle between the two para axes found from the fitting was in good agreement with that calculated by DFT (8°, in this case), and therefore, this value was kept fixed in the successive fittings. The quality of the global fitting was only slightly worse than that for the single rings: deviations were always less than 4 and 6 ppm for the $^{13}C$ and $^{19}F$ chemical shifts, respectively, amd they were less than 350 and 200 Hz for the $^{13}C-^{19}F$ and $^{1}H-^{19}F$ couplings, respectively. In this case, it must be pointed out that the introduction of $D_{ij}^{exp}$ into the set of fitted experimental data was fundamental to obtaining a good determination of the position of the principal order axis $z_{mol}$. Indeed, when chemical shifts only were used, the best value for $\alpha$ was found to be $-5.5°/-7°$, whereas this value was 2° when dipolar couplings only were used, and it was similar (4°) when all of the available data were simultaneously used in the fitting. By looking at the experimental data obtained from $^{19}F$ spectra, it was found that the $^{1}H-^{19}F$ splittings were in perfect agreement with $^{13}C-^{19}F$ splittings, whereas the $^{19}F$ chemical shift anisotropies, as in the case of 5DBF1, induced a marked increase in the deviations between the experimental and calculated data. Moreover, the deviations for $^{19}F$ chemical shifts were always systematically dependent on temperature. The orientational order parameters obtained when all of the experimental data were used in a global fitting were values of $S_{zz}$ ranging from 0.449 to 0.659 (see Figure 3) and biaxiality ranging between 0.06 and 0.07, with the $z_{mol}$ axis found to form angles of $\alpha = 4°$ and $\beta = -4°$. It must be noticed that $S_{zz}$ was very similar to the value obtained for 5DBF1 in its nematic phase, whereas in this case, we observed a non-negligible, albeit quite small, biaxiality, due to the presence of a fluorine atom in position 6, breaking the cylindrical symmetry of the molecule. The position of $z_{mol}$ was also slightly affected by the presence of this fluorine atom and, perhaps, by the shorter aliphatic chain: In 4DBF2, it was found to lie in the middle of the angle between the two para axes, whereas in 5DBF1, it was slightly more aligned with the para axis of ring B.

Some general considerations, holding true for both liquid crystals, can be drawn: The availability of a large set of experimental data, mostly due to the presence of one or two fluorine atoms on the aromatic rings, allowed for an accurate determination of the orientational order parameters and the position of the principal axis of order for the aromatic core. Nonetheless, the use of restricted subsets of experimental data for both rings always gave very similar results, with maximum differences in $S_{zz}$ of 4%, indicating a substantial robustness of the method. Only in the case of 4DBF2 was the use of $D_{ij}^{exp}$ found to be very important to obtaining a reliable determination of the order molecular axis position. The substantial agreement between the results obtained from $D_{ij}^{exp}$ and $^{13}C$ chemical shift anisotropies provides indirect validation of the appropriateness of the assumptions made in the two cases, particularly in relation to the use of vibrational corrections and DFT-optimized geometries for dipolar couplings and of DFT-calculated chemical shift tensors for chemical shift anisotropies. The imperfect agreement of the $^{19}F$ chemical shift anisotropies with the rest of the data can be ascribed to a larger experimental error in the measurement of $\delta^{obs}$ for quite broad signals (up to 1500 Hz), as well as in the determination of $\delta^{aniso}$, due to the fact that a dependence of the $\delta^{iso}$ value on temperature and phase cannot be excluded for $^{19}F$, a nucleus that is particularly sensitive to its local environment.[34,35] An additional source of error could arise from DFT calculations of $^{19}F$ chemical shift tensors; in fact, whereas DFT calculations can be considered, at present, to be a well-established method for determining $^{13}C$ chemical shift tensors, as also indicated by comparisons with experimental data,[36] the same cannot be said for $^{19}F$. The facts that the $^{19}F$ nuclei have a higher polarizability and are more exposed to the solvent than the $^{13}C$ nuclei render these nuclei more sensitive to the medium dielectric permittivity, as observed in the present

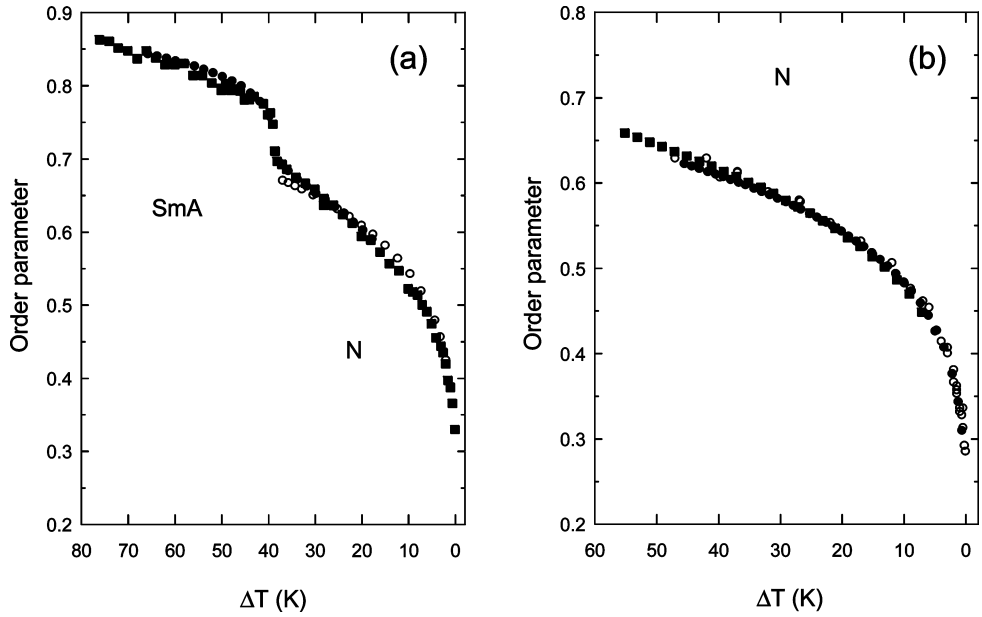


**Figure 11.** Order parameter vs shifted temperature for (a) 5DBF1 and (b) 4DBF2 after normalization to the NMR value at $\Delta T = 32$ K (normalization factors are 0.977 for $\Delta\varepsilon$ and 1.108 for $\Delta n$) and $\Delta T = 40$ K (normalization factor is 0.913 for both $\Delta\varepsilon$ and $\Delta n$), respectively. Symbols are as in Figure 3.

study passing from the in vacuo (data not shown) to the IEF-PCM calculations (further details will be provided in a future work), as well as to the C−F bond length, which can be altered during low- and high-frequency vibrational motion, corresponding to the out-of-plane bending and stretching modes, respectively.[37]

## Discussion

The orientational order parameters obtained by the three techniques employed in this work, namely, optical birefringence and dielectric permittivity measurements and multinuclear magnetic resonance spectroscopy, are summarized in Figure 3; however, before these results can be compared, a critical discussion of the differences in both the experimental and theoretical approaches used in the three methods is required. First, it is worth remembering that the different anisotropic quantities measured imply different frames of reference for the determined order parameters. In particular, optical and dielectric methods measure whole-molecule quantities and, therefore, determine a molecular order parameter relative to the principal axis of the polarizability and dielectric tensors, respectively, the biaxiality being considered null by virtue of the molecule and phase symmetries. On the contrary, NMR observables provide access to local orientational order parameters relative to molecular fragments, with the number of independent parameters being determined by the phase and fragment symmetries. In the present case, two order parameters ($S_{zz}$ and $S_{xx} - S_{yy}$) relative to frames located in the two aromatic rings separately and in the whole aromatic core were determined; the $S_{zz}$ values obtained in the last case are reported in Figure 3. Moreover, whereas NMR data allow order parameters to be determined independently at each temperature, optical and dielectric measurements require the assumption of a suitable model for describing the trend of the order parameter with temperature. In addition, in the dielectric anisotropy data analysis, it was assumed that the Maier and Meier equation (eq 3) can be reduced to a simplified relation between $\Delta\varepsilon$ and the order parameter, neglecting the temperature dependence of the density and the polarization anisotropy of the mesogens. These assumptions are, however, well fulfilled in the case of strongly polar compounds such as those examined in this work. In the analysis of the optical birefringence, instead, the local field problem was overcome by applying an empirical formula proposed by Haller for normalization of polarizabilities, leading to eq 1. On the contrary, the large set of data available from $^{13}$C and $^{19}$F experiments allowed a quite refined analysis (see Results section), as well as a critical evaluation of the influence of the set of experimental observables used on the obtained parameters, taking into account both the experimental errors and the assumptions required. In particular, in the analysis of the $^{13}$C−$^{19}$F and $^{1}$H−$^{19}$F couplings, errors can arise from the assumed geometrical data, here taken from geometry optimization at the DFT level. Moreover, contributions to the couplings arising from the anisotropic scalar interaction and possible deformations of the geometry due to harmonic vibrations were empirically estimated for the $^{13}$C−$^{19}$F couplings and neglected for the $^{1}$H−$^{19}$F coupling, whereas additional contributions due to geometry deformation related to both anharmonic vibrations and anisotropic forces of the solvent molecules were neglected in all cases on the basis of either theoretical or experimental data reported in the literature for analogous systems. Therefore, even though this analysis can be considered quite reliable, systematic errors in the order parameter determination could arise from the absence of a more refined vibrational analysis. On the other hand, in the analysis of $^{13}$C and $^{19}$F chemical shift anisotropies, two main sources of error can be identified: The first derives from the fact that the same value of isotropic chemical shift ($\delta^{iso}$) was used at all temperatures to calculate $\delta^{aniso}$ from $\delta^{obs}$; the second is related to the values used for chemical shift tensor components and the location with respect to the molecular reference frames, here calculated using DFT methods. For $^{13}$C, the use of advanced DFT methods, also including the medium effect, and the experimentally verified weak dependence of $\delta^{iso}$ on temperature render the adopted procedure quite reliable. The same cannot be safely said for $^{19}$F data because of the higher sensitivity of the fluorine nucleus to its environment, resulting

in both a non-negligible dependence of the isotropic chemical shift on temperature and less reliable chemical shift tensor calculations.

Considering all of this information, the principal order parameters obtained by the three methods can be compared. As shown in Figure 3a, in the case of 5DBF1, NMR and dielectric data gave very similar results in the N phase, whereas a smaller parameter was determined from birefringence measurements. In the case of 4DBF2 (Figure 3b), instead, the dielectric and optical measurements gave essentially the same order parameter at all temperatures, whereas a smaller parameter was determined by NMR data analysis. Resorting to a normalization procedure already employed in previous works,[6,7] the $S_{zz}$ parameters determined by NMR can be considered as reference data for the order parameters obtained by the other methods; by applying a scaling factor independent of temperature to the order parameters from optical and dielectric methods in order to obtain the best superposition of the NMR $S_{zz}$ trends, the results shown in Figure 11 are obtained, with scaling factors as reported in the figure caption. Also, considering that the biaxiality determined via NMR analysis is negligibly small, these results indicate that, for 5DBF1, the principal order axis, $z_{mol}$, located on the aromatic core as found from the NMR data analysis ($z_{mol}$ forms angles of $\alpha = -7°$ and $\beta = 4°$ with the para axes of rings A and B, respectively) is very close to the principal order axis for the dielectric tensor, but not to that of the polarizability tensor; from the scaling factors, angles of 7° and 15° can be estimated between the NMR $z_{mol}$ axis and the principal axis of the dielectric and polarizability tensors, respectively. In the case of 4DBF2, the principal axis of the dielectric and polarizabilty tensors seem to be coincident, and an angle of 14° is estimated between them and the $z_{mol}$ axis (forming angles of $\alpha = 4°$ and $\beta = -4°$ with the para axes of rings A and B, respectively), although the biaxiality found from NMR spectroscopy is not negligible. Moreover, for both mesogens, the trends with temperature of the order parameters determined by the different methods are in very good agreement.

## Conclusions

In this work, a detailed analysis of the orientational order of two fluorinated liquid crystals containing the 1,3,2-dioxaborinane ring was performed by means of optical, dielectric, and NMR spectroscopies. In the case of NMR spectroscopy, data from both $^{13}C$ and $^{19}F$ experiments were exploited, including dipolar couplings and chemical shift anisotropies, and analyzed using advanced DFT methods. For the NMR results, nuclear parameters arising from $^{13}C$ spectra (chemical shift anisotropies and $^{13}C-^{19}F$ couplings) showed good agreement, whereas larger errors were found for $^{19}F$ chemical shift anisotropies, which were ascribed to both experimental and theoretical sources. The trends with temperature of the principal order parameters determined from the different methods, although referred to different frames, are in very good agreement. The relative location of the principal order axes could be estimated using a normalization procedure, and possible errors and assumptions related to the different experimental and theoretical methods employed were analyzed and discussed.

**Acknowledgment.** This work was partially supported by the executive program of scientific and technological co-operation between the Italian Republic and the Republic of Poland 2007−2009 (Project No. 8). Giulia Mollica is thanked for her help in $^{13}C$ NMR measurements.

## References and Notes

(1) Virchow, R. *Angew. Chem., Int. Ed.* **2000**, *39*, 4216.
(2) Kirsch, P.; Huber, F.; Lenges, M.; Taugerbeck, A. *J. Fluorine Chem.* **2001**, *112*, 69.
(3) Hird, M. *Chem. Soc. Rev.* **2007**, *36*, 2070.
(4) Dabrowski, R.; Bezborodov, V. S.; Lapanik, V. J.; Dziaduszek, J.; Czupryński, K. *Liq. Cryst.* **1995**, *18*, 213.
(5) Czub, J.; Dabrowski, R.; Urban, S. *Phase Trans.* **2007**, *80*, 631.
(6) Catalano, D.; Geppi, M.; Marini, A.; Veracini, C. A.; Urban, S.; Czub, J.; Kuczyński, W.; Dabrowski, R. *J. Phys. Chem. C* **2007**, *111*, 5286.
(7) Geppi, M.; Marini, A.; Veracini, C. A.; Urban, S.; Czub, J.; Kuczyński, W.; Dabrowski, R. *J. Phys. Chem. B* **2008**, *112*, 9663.
(8) Veracini C. A. In *Nuclear Magnetic Resonance of Liquid Crystals*; Emsley, J. W., Ed.; Reidel Publishing Company: Dordrecht, Germany, 1985; pp 99−121.
(9) Emsley, J. W. In *Nuclear Magnetic Resonance of Liquid Crystals*; Emsley, J. W., Ed.; Reidel Publishing Company: Dordrecht, Germany, 1985; pp 379−412.
(10) Dong, R. Y. *Nuclear Magnetic Resonance of Liquid Crystals*; Springer Verlag Inc.: New York, 1994.
(11) Tomasi, J. Modern Theories of Continuum Models. In *Continuum Solvation Models in Chemical Physics: Theory and Applications*; Mennucci, B., Cammi, R., Eds.; John Wiley and Sons, Ltd.; Chichester, U.K., 2007; Chapter 1.
(12) Cancès, E.; Mennucci, B.; Tomasi, J. *J. Chem. Phys.* **1997**, *107*, 3032.
(13) Kuczyński, W.; Żywucki, B.; Malecki, J. *Mol. Cryst. Liq. Cryst.* **2002**, *381*, 1.
(14) Fung, B. M.; Khitrin, A. K.; Ermolaev, K. *J. Magn. Reson.* **2000**, *142*, 97.
(15) Frisch, M. J.; Trucks, G. W.; Schlegel, H. B.; Scuseria, G. E.; Robb, M. A.; Cheeseman, J. R.; Montgomery, J. A., Jr.; Vreven, T.; Kudin, K. N.; Burant, J. C.; Millam, J. M.; Iyengar, S. S.; Tomasi, J.; Barone, V.; Mennucci, B.; Cossi, M.; Scalmani, G.; Rega, N.; Petersson, G. A.; Nakatsuji, H.; Hada, M.; Ehara, M.; Toyota, K.; Fukuda, R.; Hasegawa, J.; Ishida, M.; Nakajima, T.; Honda, Y.; Kitao, O.; Nakai, H.; Klene, M.; Li, X.; Knox, J. E.; Hratchian, H. P.; Cross, J. B.; Bakken, V.; Adamo, C.; Jaramillo, J.; Gomperts, R.; Stratmann, R. E.; Yazyev, O.; Austin, A. J.; Cammi, R.; Pomelli, C.; Ochterski, J. W.; Ayala, P. Y.; Morokuma, K.; Voth, G. A.; Salvador, P.; Dannenberg, J. J.; Zakrzewski, V. G.; Dapprich, S.; Daniels, A. D.; Strain, M. C.; Farkas, O.; Malick, D. K.; Rabuck, A. D.; Raghavachari, K.; Foresman, J. B.; Ortiz, J. V.; Cui, Q.; Baboul, A. G.; Clifford, S.; Cioslowski, J.; Stefanov, B. B.; Liu, G.; Liashenko, A.; Piskorz, P.; Komaromi, I.; Martin, R. L.; Fox, D. J.; Keith, T.; Al-Laham, M. A.; Peng, C. Y.; Nanayakkara, A.; Challacombe, M.; Gill, P. M. W.; Johnson, B.; Chen, W.; Wong, M. W.; Gonzalez, C.; Pople, J. A. *Gaussian 03*, revision B05; Gaussian, Inc.: Pittsburgh, PA, 2004.
(16) *CS MOPAC Pro*; CambridgeSoft: Cambridge, MA, 1999.
(17) Ditchfield, R. *J. Chem. Phys.* **1972**, *56*, 5688.
(18) Gauss, J. *J. Chem. Phys.* **1993**, *99*, 3629.
(19) Perdew, J. P. In *Electronic Structure of Solids*; Ziesche, P., Eschig, H., Eds.; Akademie Verlag: Berlin, 1991.
(20) Adamo, C.; Barone, V. *J. Chem. Phys.* **1998**, *108*, 664.
(21) Cheeseman, J. R.; Trucks, G. W.; Keith, T. A.; Frisch, M. J. *J. Chem. Phys.* **1998**, *104*, 5497.
(22) Żywucki, B.; Kuczyński, W.; Czechowski, G. *Proc. SPIE Int. Soc. Opt. Eng.* **1995**, *2372*, 151–156.
(23) Maier, W.; Meier, G. *Z. Naturforsch. A* **1961**, *16* (262), 470.
(24) Kresse, H. *Adv. Liq. Cryst.* **1983**, *6*, 109.
(25) Urban, S.; Gestblom, B.; Pawlus, S. *Z. Naturforsch. A* **2003**, *58*, 357.
(26) Czub, J.; Urban, S.; Würflinger, A. *Liq. Cryst.* **2006**, *33*, 85.
(27) Dunmur, D. A. *Liq. Cryst.* **2005**, *32*, 1379.
(28) Haller, I. V. *Prog. Solid State Chem.* **1975**, *10*, 103.
(29) Urban, S.; Gestblom, B.; Würflinger, A. *Phys. Chem. Chem. Phys.* **1999**, *1*, 2787, and references therein.
(30) Abragam, A. *The Principles of Nuclear Magnetism*; Oxford University Press: London, 1961.
(31) Vaara, J.; Jokisaari, J.; Wasylishen, R. E.; Bryce, D. L. *Prog. Nucl. Magn. Reson. Spectrosc.* **2002**, *41*, 233.
(32) Vaara, J.; Kaski, J.; Jokisaari, J. *J. Phys. Chem. B* **1999**, *103*, 5675.
(33) Lucas, N. J. *Mol. Phys.* **1971**, *22*, 233.
(34) Brey, W. S.; Brey, M. L. In *Encyclopedia of Nuclear Magnetic Resonance*; Grant, D. M. , Harris, R. K., Eds.; Wiley: Chichester, U.K. 1996; pp 2063−2071.
(35) Ulrich, A. S. *Prog. Nucl. Magn. Reson. Spectrosc.* **2005**, *46*, 1.
(36) Dong, R. Y.; Geppi, M.; Marini, A.; Hamplova, V.; Kaspar, M.; Veracini, C. A.; Zhang, J. *J. Phys. Chem. B* **2007**, *111*, 9787.
(37) Sanders, L. K.; Oldfield, E. *J. Phys. Chem. A* **2001**, *105*, 8098.

JP908241N